Control of topological phase transitions in Dirac semimetal films by exchange fields*

Fei Yang(杨菲), Hai-Long Wang(王海龙)†, and Hui Pan(潘晖)‡

Department of Physics, Beihang University, Beijing 100191, *China*

(Received 5 July 2016; revised manuscript received 22 October 2016; published online 22 December 2016)

The exchange field effects on topological Dirac semimetal (DSM) films are discussed in this article. A topological phase transition can be controlled by tuning the exchange field together with the quantum confinement effects. What is more interesting is that the system can transit into the quantum anomalous Hall (QAH) state from the topologically trivial state ($\mathbb{Z}_2 = 0$) or from the topologically nontrivial state ($\mathbb{Z}_2 = 1$), depending on the thickness of the DSM films. This provides a useful mechanism to realize the QAH state from the DSM.

Keywords: exchange field, Dirac semimetal, quantum anomalous Hall state, quantum spin Hall state

PACS: 71.20.–b, 73.20.At, 73.22.Gk, 73.43.Nq **DOI:** 10.1088/1674-1056/26/1/017102

1. Introduction

Topological insulators are hot topics in the study of condensed matter physics.[1,2] The topological insulators with time-reversal symmetry (TRS) can be classified by a $\mathbb{Z}_2$ topological parameter. In these topological insulators, the gapless states in surface or edge are protected by TRS, and these topologically nontrivial states have a nonzero topological number $\mathbb{Z}_2$.[1–3] The nontrivial topology state, known as the quantum spin Hall (QSH) state,[4–7] is labeled by the integer $\mathbb{Z}_2 = 1$.

When the TRS is broken, the quantum anomalous Hall (QAH) states can be realized in a system with strong spin–orbit coupling (SOC), where no orbital magnetic field and Landau levels exist.[8–10] In the QAH states, the gapless edge modes at the boundaries have a well-defined topological order in the bulk, which is characterized by the first Chern number $\mathcal{C}$.[11–13] The QAH is expected to exist in graphene with the effects of the Rashba spin–orbit coupling and exchange field, and also in the hybrid model with the doping transition-metal atoms.[14–18] Just recently, a new theory has been proposed that the QAH can be obtained by n–p codoping in three-dimensional topological insulators at high temperatures.[19] The discovery of the QAH effect makes it possible for topological materials to realize the electronics with very low energy dissipation, and it also brings a broader prospect for the novel quantum devices' application.[20,21] Moreover, the experiments on topology with magnetic semimetal have realized the QAH,[22–25] which greatly promotes the study of topological insulator.

Besides the research and development of topological insulators, the topology of semimetal research has also entered a new stage. Dirac semimetal (DSM) has been known as a kind of topological semimetal, which has topological properties but without a bulk band gap. This kind of material is difficult to obtain, but recent experiments have found it, such as Na_3Bi and Cd_3As_2.[26–34] The Fermi surface of this kind of material is preserved by the crystalline symmetry and has four-fold degenerate Dirac point(s).[35] Each Dirac point can be viewed as two opposite chiral Weyl points' superposition, which is protected by the lattice symmetry.[36–39] The DSM can be viewed as a parent material to realize the topological insulators. If the DSM sample has a finite thickness in some fixed direction, the coupling in the two surface states will produce a gap at the Dirac points and realize a QSH phase.[35,40] In the DSM film system, a QSH phase can be obtained by the control of a vertical electric field too.[36]

In this work, the control of DSM's topological phase transitions with the exchanged field are discussed in detail. Due to the quantum confinement effects, the DSM films can be in the topologically trivial state with $\mathbb{Z}_2 = 0$ or in a topologically nontrivial state with $\mathbb{Z}_2 = 1$. With the help of exchange fields, the DSM films can be transited into the topological QAH state from the topology trivial state or from the topologically nontrivial state.

2. Physical model

The generic low-energy effective model is the base to analyse, and this model is derived from previous works for DSM A_3Bi (A = Na, K, and Rb) and Cd_3As_2.[36,41–43] As for these materials, their states can be expanded around Fermi energy by using a minimal four-orbital basis, which are $|S_{1/2}, 1/2\rangle$, $|P_{3/2}, 3/2\rangle$, $|S_{1/2}, -1/2\rangle$, and $|P_{3/2}, -3/2\rangle$. In the Brillouin zone, the effective Hamiltonian around Γ-point can

*Project supported by the National Natural Science Foundation of China (Grant No. 11574019).

†Corresponding author. E-mail: hlwang@buaa.edu.cn

‡Corresponding author. E-mail: hpan@buaa.edu.cn

© 2017 Chinese Physical Society and IOP Publishing Ltd

be expanded up to quadratic order, and in the wave-vector k direction it can be written as

$$\mathcal{H}_0(\boldsymbol{k}) = \varepsilon_0(\boldsymbol{k}) + \begin{bmatrix} M(\boldsymbol{k}) & Ak_+ & 0 & 0 \\ Ak_- & -M(\boldsymbol{k}) & 0 & 0 \\ 0 & 0 & M(\boldsymbol{k}) & -Ak_- \\ 0 & 0 & -Ak_+ & -M(\boldsymbol{k}) \end{bmatrix}, \quad (1)$$

where $\varepsilon_0(\boldsymbol{k}) = C_0 + C_1 k_z^2 + C_2(k_x^2 + k_y^2)$, $k_\pm = k_x \pm \mathrm{i}k_y$, and $M(\boldsymbol{k}) = -M_0 + M_1 k_z^2 + M_2(k_x^2 + k_y^2)$, and M_0, M_1, $M_2 > 0$, which is in order to reproduce the band inversion feature at Γ-point. By the first-principles calculation and the experimental measurement, the material-specific parameters A, C_i, and M_i can be achieved. This model captures the essential low-energy physics compared well with experiments.[26,30,35,44] The energy eigenvalue is $E(k) = \varepsilon_0(\boldsymbol{k}) \pm \sqrt{M(\boldsymbol{k})^2 + A^2(k_x^2 + k_y^2)}$. Then the coordinates of the two Dirac points in k_z-axis are $(0, 0, \pm k_\mathrm{D})$, where $\pm k_\mathrm{D} = \sqrt{M_0/M_1}$. Each Dirac point can be viewed as two opposite chiral Weyl points' superposition and it is four-fold degenerate. In the low-energy model, when DSM is confined along different directions, one can see the different anisotropic spectrums.

The exchange field's Hamiltonian can be written as

$$\mathcal{H}_h = h_1 \sigma_z \otimes \sigma_z + h_2 \sigma_z \otimes \sigma_0, \quad (2)$$

where h_1,h_2 are the exchange field strengths. Then the Hamiltonian of the system is

$$\mathcal{H}(k) = \mathcal{H}_0(\boldsymbol{k}) + \mathcal{H}_h. \quad (3)$$

In order to make the calculation for DSM with finite thickness, the model is placed in the three-dimensional (3D) lattice space. The following standard substitutions are taken

$$k_i = \frac{1}{a_i}\sin(k_i a_i), \quad k_i^2 = \frac{2}{a_i^2}[1 - \cos(k_i a_i)], \quad (4)$$

where $i = x, y, z$. Then the 3D lattice space's low-energy effective Hamiltonian around Γ in the Brillouin zone can be written as

$$\begin{aligned} H \;=\; & \sum c_i^\dagger \boldsymbol{T}_0 c_i + \sum c_i^\dagger \boldsymbol{T}_x c_{i+x} + \sum c_i^\dagger \boldsymbol{T}_y c_{i+y} \\ & + \sum c_i^\dagger \boldsymbol{T}_z c_{i+z} + \mathrm{H.c.}, \end{aligned} \quad (5)$$

where

$$\boldsymbol{T}_0 = \begin{bmatrix} M_+ + h_1 + h_2 & 0 & 0 & 0 \\ 0 & M_- + h_2 - h_1 & 0 & 0 \\ 0 & 0 & M_+ - (h_1 + h_2) & 0 \\ 0 & 0 & 0 & M_- - (h_2 - h_1) \end{bmatrix}, \quad (6)$$

$$\boldsymbol{T}_x = \begin{bmatrix} -C_2^a + M_2^a & -\frac{A^a}{2}\mathrm{i} & 0 & 0 \\ -\frac{A^a}{2}\mathrm{i} & -C_2^a - M_2^a & 0 & 0 \\ 0 & 0 & -C_2^a + M_2^a & \frac{A^a}{2}\mathrm{i} \\ 0 & 0 & \frac{A^a}{2}\mathrm{i} & -C_2^a - M_2^a \end{bmatrix}, \quad (7)$$

$$\boldsymbol{T}_y = \begin{bmatrix} -C_2^a + M_2^a & \frac{A^a}{2} & 0 & 0 \\ -\frac{A^a}{2} & -C_2^a - M_2^a & 0 & 0 \\ 0 & 0 & -C_2^a + M_2^a & \frac{A^a}{2} \\ 0 & 0 & -\frac{A^a}{2} & -C_2^a - M_2^a \end{bmatrix}, \quad (8)$$

$$\boldsymbol{T}_z = \begin{bmatrix} -C_1^a + M_1^a & 0 & 0 & 0 \\ 0 & -C_1^a - M_1^a & 0 & 0 \\ 0 & 0 & -C_1^a + M_1^a & 0 \\ 0 & 0 & 0 & -C_1^a - M_1^a \end{bmatrix}. \quad (9)$$

Here $M_\pm = C_0 \pm M_0 + (2C_1^a + 4C_2^a) \mp (2M_1^a + 4M_2^a)$.

In order to study the topological nature further, the local density of states (LDOS) by using the iterative method of Green function $\rho(k_i) = -\mathrm{Tr}[\mathrm{Im}\boldsymbol{G}_{00}(k_i)]/\pi$ is calculated, where $\boldsymbol{G}_{00}$ is the delayed function of the lattice surface. $\boldsymbol{G}_{00}$ can be calculated by transfer matrix

$$\boldsymbol{G}_{00} = (\boldsymbol{E} - \boldsymbol{H}_{00} - \boldsymbol{H}_{01}\boldsymbol{T})^{-1}, \quad (10)$$

$$\boldsymbol{T} = (\boldsymbol{E} - \boldsymbol{H}_{00} - \boldsymbol{H}_{01}\boldsymbol{T})^{-1}\boldsymbol{H}_{01}^\dagger, \quad (11)$$

where $\boldsymbol{H}_{00}$ and $\boldsymbol{H}_{01}$ are Hamiltonian matrixes, and $\boldsymbol{T}$ is inverse matrix. Then the surface LDOS is obtained.

3. Numerical results and discussion

In the numerical calculations, parameters of Na_3Bi are taken as follows. The thickness of Na_3Bi thin films l is limited along z direction and the lattice constants are taken as $a_x = a_y = 0.5448$ nm, $a_z = 0.4828$ nm. The adopted constants are related to the separation between internal layer of DSM. The other calculation parameters for Na_3Bi are $C_0 = -63.82$ meV, $C_1 = 87.536$ meV$\cdot$nm^2, $C_2 = -84.008$ meV$\cdot$nm^2, $M_0 = 86.86$ meV, $M_1 = 106.424$ meV$\cdot$nm^2, $M_2 = 103.610$ meV$\cdot$nm^2, and $A = 245.98$ meV$\cdot$nm, which are determined by the first-principles calculations and experiments.[26,38]

The case where the film's layer $l = 5$ is discussed first. It can be seen from Fig. 1(a) that, where the exchange field h_2 is set to be 0, the energy gap is changing with the exchange field h_1. When $h_1 = 0$, the diagram shows that the system has

a gap about 70 meV, which is marked as A point in Fig. 1(a). With the increase of h_1, energy gap decreases and closes at $h_1 = 27$ meV, which is marked as B point. Then with the increase of h_1, the gap reopens. The energy spectrums shown in Figs. 1(b)–1(d) correspond to the three states marked by A, B, and C in Fig. 1(a), respectively. The parameters are $h_1 = 0$, $h_2 = 0$ for Fig. 1(b), $h_1 = 35$ meV, $h_2 = 0$ for Fig. 1(c), and $h_1 = 75$ meV, $h_2 = 0$ for Fig. 1(d). All the points are plotted versus k_x (with $k_y = 0$). We can see that before the closing point, the system has a gap, which belongs to the insulating state; after the closing point the system is also in the insulation state. Thus the critical closing point divides the topological phase into a topologically trivial phase and a nontrivial phase.

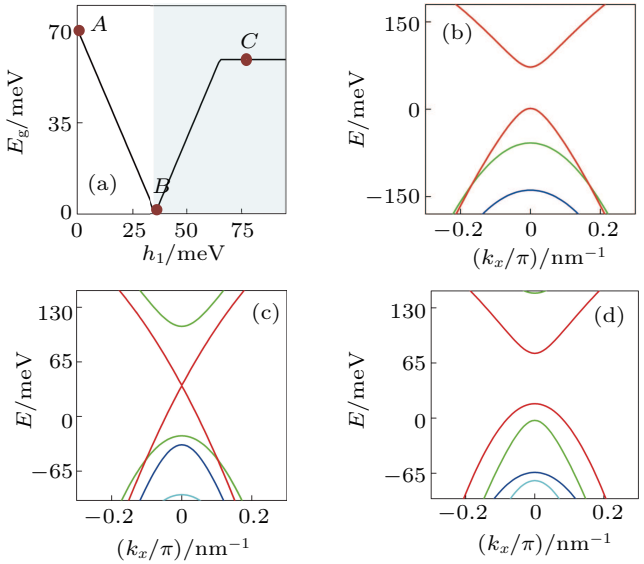


Fig. 1. (color online) The influence of exchange field on edge states. (a) Energy gap as a function of the exchange field h_1. Energy spectrums corresponding to points A (b), B (c), and C (d) in panel (a) are plotted versus k_x (with $k_y = 0$). The first three sub-bands are labeled with red, green, and blue colors, respectively. The parameters used in the calculation are $h_2 = 0$ and the thickness of Na_3Bi thin films $l = 5$.

Then, the LDOS to observe the edge states' variation is calculated, known as $\rho(k_x) = -\mathrm{Tr}[\mathrm{Im}\boldsymbol{G}_{00}(k_x)]/\pi$. As we all know, in the low energy model, the $k_x - k_y$ plane has the nature of the isotropic. So without loss of generality, the phase diagram along x direction is only discussed.[36] Here the system has a confinement along z direction.

When the thin film's layer $l = 5$, the surface LDOS corresponding to the point A and C in Fig. 1(a) are shown in Fig. 2. Figures 2(a) and 2(b) represent the states before and after the closing point, respectively. The energy gap can be identified clearly. Before the closing point, there are no edge states between the energy gap and it is a trivial insulator state; but after the closing point, there appears a bright line between the energy gap and it is crossing the gap. This is corresponding to the QAH phase.

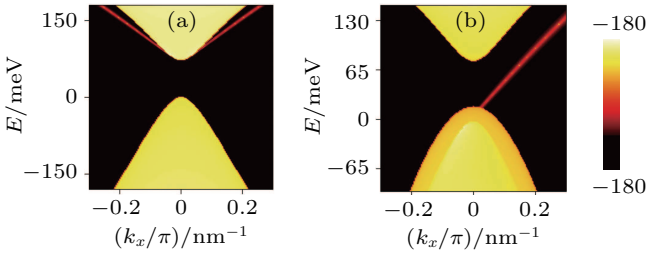


Fig. 2. (color online) The surface local density of states (LDOS) with $l = 5$, corresponding to the points A (a) and C (b) in Fig. 1(a). (a) The trivial insulator state, where there is no edge state in the gap. (b) The QAH state, where one edge state exists in the gap. The parameters used in panels (a) and (b) are the same as those in Figs. 1(b) and 1(d), respectively.

For a more comprehensive analysis of the spectrum, the energy spectrum's phase diagrams are calculated. The phase diagram with $l = 5$ is shown in Fig. 3. It can be seen that the film's energy spectrum has a gap at point A in Fig. 3, corresponding to point A in Fig. 1(a), and it is a trivial insulator. Point B in Fig. 3 is correctly the echo of point B in Fig. 1(a), where the film's energy spectrum is gapless. Point C in Fig. 3 is also corresponding to the point C in Fig. 1(a), which is the QAH phase.

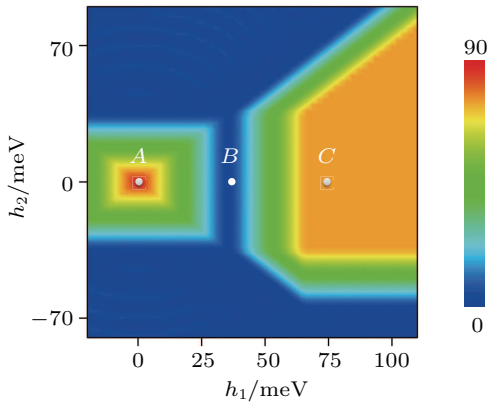


Fig. 3. (color online) Phase diagram with $l = 5$. Band gap is numerically obtained as a function of h_1 and h_2. Color measures the size of the band gap. The white points agree well with the points in Fig. 1(a).

Next, the case where the film's layer $l = 7$ is discussed. It can be seen from Fig. 4(a) that, when the exchange field h_2 is set to be 10 meV, the energy gap is changing with the exchange field h_1 . When $h_1 = 0$, the system has a gap about 14 meV as shown in Fig. 4(a), which is marked as A point. With the increase of h_1, the energy gap decreases and closes at $h_1 = 17$ meV, which is marked as B point. Then with the increase of h_1, the gap reopens. The energy spectrums shown in Figs. 4(b)–4(d) correspond to the three states marked by A, B, and C in Fig. 4(a) in turn. The parameters are $h_1 = 0$, $h_2 = 10$ meV for Fig. 4(b), $h_1 = 17$ meV, $h_2 = 10$ meV for Fig. 4(c), and $h_1 = 40$ meV, $h_2 = 10$ meV for Fig. 4(d). All the points are plotted versus k_x (with $k_y = 0$). It can be seen that before the closing point, the system has a gap, but there are a pair of edge states in the gap, which belongs to the QSH

state. After the closing point, the system is also in the insulation state. While there appears an edge state in the gap, this is a QAH state.

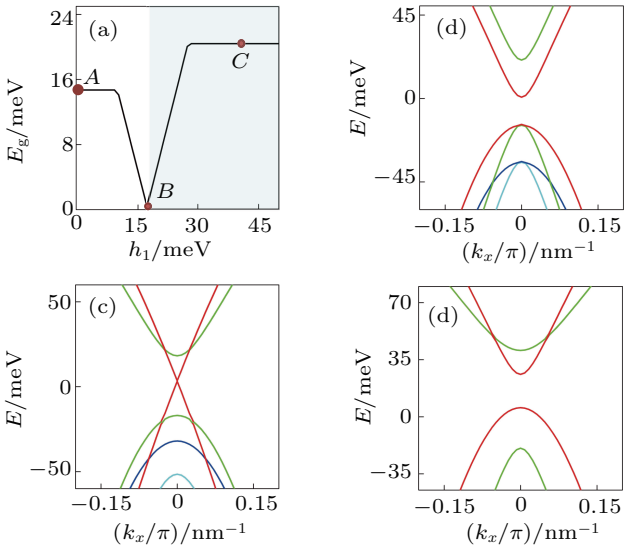


Fig. 4. (color online) The influence of exchange field on edge states. (a) Energy gap as a function of the exchange field h_1. It can be seen that the energy gap has a process from closing to opening. Energy spectrums corresponding to points A (b), B (c), and C (d) in panel (a) are plotted versus k_x (with $k_y = 0$). The first three sub-bands are striped with red, green, and blue colors, respectively. The parameters used in the calculation are $h_2 = 10$ meV and $l = 7$.

The corresponding LDOS of the point A and C in Fig. 4(a) are shown in Fig. 5. Figures 5(a) and 5(b) represent the state before and after the closing point B, respectively. It can be seen that the energy gaps are identified clearly. Before the closing point, there are a pair of edge states crossing the gap and it is a QSH state, but after the closing point, there appears only a bright line between the energy gap and it is crossing the gap. This is corresponding to the QAH phase.

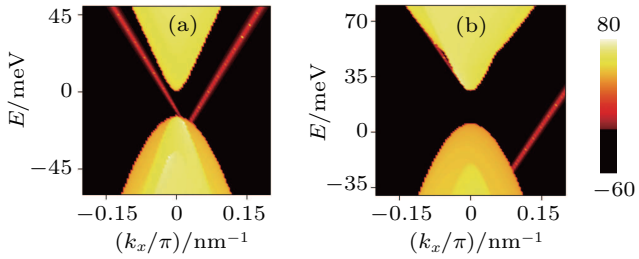


Fig. 5. (color online) The surface local density of states (LDOS) with $l = 7$, correspond to the points A (a) and C (b) in Fig. 4(a). (a) There are a pair of edge states crossing the gap, which is a QSH state. (b) There is an edge state in the gap, which represents that it is a QAH state. The parameters used in panels (a) and (b) are the same as those in Figs. 4(b) and 4(d), respectively.

Finally, the phase diagram with $l = 7$ is calculated, shown in Fig. 6. It can be seen that the film's energy spectrum opens a gap at point A in Fig. 6, which is corresponding to point A in Fig. 4(a), and there are a pair of edge states crossing the gap, which is a QSH phase. Point B in Fig. 6 is correctly the echo of point B in Fig. 4(a), where the film's energy spectrum is gapless. Point C in Fig. 6 is also corresponding to the C point in Fig. 4(a), which is the QAH phase.

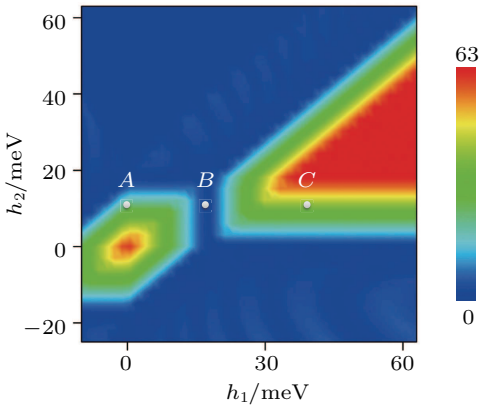


Fig. 6. (color online) Phase diagram with $l = 7$. Band gap is numerically obtained as a function of h_1 and h_2. Color measures the size of the band gap. The white points overlap with the points in Fig. 4(a).

4. Conclusion

The exchange field effects on topological DSM films are studied in detail. It is found that a topological phase transition can be controlled by tuning the exchange field together with the quantum confinement effects. The DSM file exhibits different topological properties for different thickness, i.e., BI for $l = 5$ with $\mathbb{Z}_2 = 0$, while QSH state for $l = 7$ with $\mathbb{Z}_2 = 1$. It is interesting to find that the system can transit into the QAH state with nonzero C from the topologically trivial state ($\mathbb{Z}_2 = 0$) or from the topologically nontrivial state ($\mathbb{Z}_2 = 1$). This provides a useful mechanism to realize the QAH state from the DSM.

References

[1] Hasan M Z and Kane C L 2010 *Rev. Mod. Phys.* **82** 3045
[2] Qi X L and Zhang S C 2011 *Rev. Mod. Phys.* **83** 1057
[3] Ando Y 2013 *J. Phys. Soc. Jpn.* **82** 102001
[4] Kane C L and Mele E J 2005 *Phys. Rev. Lett.* **95** 146802
[5] König M, Wiedmann S, Brüne C, Roth A, Buhmann H, Molenkamp L W, Qi X L and Zhang S C 2007 *Science* **318** 766
[6] Schnyder A P, Ryu S, Furusaki A and Ludwig A W W 2008 *Phys. Rev. B* **78** 195125
[7] Qi X L, Wu Y S and Zhang S C 2006 *Phys. Rev. B* **74** 085308
[8] Ren Y F, Qiao Z H and Niu Q 2016 *Rep. Prog. Phys.* **79** 066501
[9] Wong H M, Yu R, Hu X, Dai X and Fang Z 2015 *Adv. Phys.* **64** 227
[10] Liu C X, Zhang S C and Qi X L 2016 *Annu. Rev. Condens. Matter Phys.* **7** 301
[11] Liu C X, Qi X L, Dai X, Fang Z and Zhang S C 2008 *Phys. Rev. Lett.* **101** 146802
[12] Laughlin R B 1981 *Phys. Rev. B* **23** 5632
[13] Thouless D J, Kohmoto M, Nightingale M P and den Nijs M 1982 *Phys. Rev. Lett.* **49** 405
[14] Qiao Z H, Ren W, Chen H, Bellaiche L, Zhang Z Y, MacDonald A H and Niu Q 2014 *Phys. Rev. Lett.* **112** 116404
[15] Qiao Z H, Yang S A, Feng W X, Tse W K, Ding J, Yao Y G, Wang J and Niu Q 2010 *Phys. Rev. B* **82** 161414
[16] Qiao Z H, Han Y L, Zhang L, Wang K, Deng X Z, Jiang H, Yang S Y, Wang J and Niu Q 2016 *Phys. Rev. Lett.* **117** 056802

[17] Zhang H B, Lazo C, Blügel S, Heinze S and Mokrousov Y 2012 *Phys. Rev. Lett.* **108** 056802

[18] Choi Y H, Jo N H, Lee K J, Yoon J B, You C Y and Jung M H 2011 *J. Appl. Phys.* **109** 07E312

[19] Qi S F, Qiao Z H, Deng X Z, Cubuk E D, Chen H, Zhu W G, Kaxiras E, Zhang S B, Xu X H and Zhang Z Y 2016 *Phys. Rev. Lett.* **117** 056804

[20] Qiao Z H, Jiang H, Li X, Yao Y G and Niu Q 2012 *Phys. Rev. B* **85** 115439

[21] Nourbakhsh Z and Vaez A 2016 *Chin. Phys. B* **25** 037101

[22] Chang C Z, Zhang J S, Feng X, Shen J, Zhang Z C, Guo M H, Li K, Ou Y B, Wei P, Wang L L, Ji Z Q, Feng Y, Ji S H, Chen X, Jia J F, Dai X, Fang Z, Zhang S C, He K, Wang Y Y, Lu L, Ma X C and Xue Q K 2013 *Science* **340** 167

[23] Nomura K and Nagaosa N 2011 *Phys. Rev. Lett.* **106** 166802

[24] Hor Y S, Roushan P, Beidenkopf H, Seo J, Qu D, Checkelsky J G, Wray L A, Hsieh D, Xia Y, Xu S Y, Qian D, Hasan M Z, Ong N P, Yazdani A and Cava R J 2010 *Phys. Rev. B* **81** 195203

[25] Kou X, Guo S T, Fan Y, Pan L, Lang M, Jiang Y, Shao Q, Nie T, Murata K, Tang J, Wang Y, He L, Lee T K, Lee W L and Wang K L 2014 *Phys. Rev. Lett.* **113** 199901

[26] Liu Z K, Zhou B, Zhang Y, Wang Z J, Weng H M, Prabhakaran D, Mo S K, Shen Z X, Fang Z, Dai X, Hussain Z and Chen Y L 2014 *Science* **343** 864

[27] Zhang Y, Liu Z K, Zhou B, Kim Y, Hussain Z, Shen Z X, Chen Y L and Mo S K 2014 *Appl. Phys. Lett.* **105** 031901

[28] Borisenko S, Gibson Q, Evtushinsky D, Zabolotnyy V, Büchner B and Cava R J 2014 *Phys. Rev. Lett.* **113** 027603

[29] Neupane M, Xu S Y, Sankar R, Alidoust N, Bian G, Liu C, Belopolski I, Chang T R, Jeng H T, Lin H, Bansil A, Chou F C and Hasan M Z 2014 *Nat.Commun.* **5** 3786

[30] Jeon S, Zhou B B, Gyenis A, Feldman B E, Kimchi I, Potter A C, Gibson Q D, Cava R J, Vishwanath A and Yazdani A 2014 *Nat. Mater.* **13** 851

[31] Liang T, Gibson Q, Ali M N, Liu M H, Cava R J and Ong N P 2015 *Nat. Mater.* **14** 280

[32] Yi H, Wang Z J, Chen C Y, Shi Y G, Feng Y, Liang A J, Xie Z J, He S L, He J F, Peng Y Y, Liu X, Liu Y, Zhao L, Liu G D, Dong X L, Zhang J, Nakatake M, Arita M, Shimada K, Namatame H, Taniguchi M, Xu Z Y, Chen C T, Dai X, Fang Z and Zhou X J 2014 *Sci. Rep.* **4** 6106

[33] He L P, Hong X C, Dong J K, Pan J, Zhang Z and Li S Y 2014 *Phys. Rev. Lett.* **113** 246402

[34] Xu S Y, Liu C, Kushwaha S K, Sankar R, Krizan J W, Belopolski I, Neupane M, Bian G, Alidoust N, Chang T R, Jeng H T, Huang C Y, Tsai W F, Lin H, Shibayev P P, Chou F C, Cava R J and Hasan M Z 2015 *Science* **347** 294

[35] Xiao X B, Yang S A, Liu Z F, Li H L and Zhou G H 2015 *Sci. Rep.* **5** 7898

[36] Pan H, Wu M M, Liu Y and Yang S A 2015 *Sci. Rep.* **5** 14639

[37] Young S M, Zaheer S, Teo J C Y, Kane C L, Mele E J and Rappe A M 2012 *Phys. Rev. Lett.* **108** 140405

[38] Wang Z J, Sun Y, Chen X Q, Franchini C, Xu G, Weng H M, Dai X and Fang Z 2012 *Phys. Rev. B* **85** 195320

[39] Wang Z J, Weng H M, Wu Q S, Dai X and Fang Z 2013 *Phys. Rev. B* **88** 125427

[40] Fu L and Kane C L 2007 *Phys. Rev. B* **76** 045302

[41] Wang Z J, Sun Y, Chen X Q, Franchini C, Xu G, Weng H M, Dai X and Fang Z 2012 *Phys. Rev. B* **85** 195320

[42] Lu Q, Zhang H Y, Cheng Y, Chen X R and Ji G F 2016 *Chin. Phys. B* **25** 026401

[43] Wang Z J, Weng H M, Wu Q S, Dai X and Fang Z 2013 *Phys. Rev. B* **88** 125427

[44] Liu Z K, Jiang J, Zhou B, Wang Z J, Zhang Y, Weng H M, Prabhakaran D, Mo S K, Peng H, Dudin P, Kim T, Hoesch M, Fang Z, Dai X, Shen Z X, Feng D L, Hussain Z and Chen Y L 2014 *Nat. Mater.* **13** 677